TriboMotion: A Self-Powered Triboelectric Motion Sensor in Wearable Internet of Things for Human Activity Recognition and Energy Harvesting

Hui Huang, Xian Li, Si Liu, Shiyan Hu, *Senior Member, IEEE*, and Ye Sun, *Member, IEEE*

***Abstract*—Human physical activity recognition is widely used in medical diagnosis, well-being management, and rehabilitation treatment. In spite of various Internet of Things (IoT) designs available in the literature, power resources often limit the lifetime of IoT. Regarding this weakness, this paper develops a new motion sensor system in wearable IoT (WIoT) for human physical activity recognition without any signal conditioning circuits. The triboelectricity-based physical model is explored in designing the motion sensor. It enables to collect motion signals caused by physical activities without any power supply. In addition, the triboelectric structure can be used as an energy harvester for motion harvesting due to its high output voltage in random low-frequency motion and a relatively stable voltage when involving continuous activities. Such a new design lays the foundations for constructing the next generation self-powered WIoT systems. Our new design has been extensively evaluated, where most common activities including sitting and standing, walking, climbing upstairs and downstairs, and running are used. The experimental results demonstrate that our system can achieve similar comparable performance as the state of the art for physical activity recognition at an average successful accuracy of over 80%. At the same time, our system reduces more than 25% energy consumption of the entire sensing hardware system which includes the sensor, microcontroller, and corresponding circuits.**

***Index Terms*—Motion energy harvesting, physical activity recognition, triboelectric, wearable Internet of Things (WIoT).**

I. Introduction

THE HIGH cost of prolonged in-hospital healthcare on chronic conditions has facilitated the human-centered out-of-hospital healthcare [1], [2]. Telemedicine and mobile health integrated with wearable sensors and systems provide a good solution for out-of-hospital healthcare with doctors in the loop to achieve efficient and effective telemedicine interventions, which has been considered as one of the most significant drivers of Internet of Things (IoT) technologies [3]. Recent progress of IoT technologies connects real world objects to Internet, which is rapidly emerging with an increasing number of Internet-enabled devices. Wearable sensors and devices are capable of continuously sensing and transmitting health related data to Internet-enabled devices for daily monitoring and well-being management, forming the emerging wearable IoT (WIoT) system [3].

In human-centered healthcare, an important technology with extensive applications is human physical activity recognition. In recent decades, it has become an active area with the exceptional development of wearable motion sensors. Power supply is one of the major challenges for continuous monitoring using these wearable motion sensors; and energy harvesting from motion is considered as a promising solution [4].

For motion harvesting, three mechanisms are commonly used, piezoelectricity based on piezoelectric materials, electromagnetics based on Lenz's law, and electrostatics based on variable capacitance [5]. Alternatively, triboelectric nanogenerators (TENGs) are a new type of mechanical energy harvesters, which are based on triboelectric and electrostatic effects enhanced by adding nano- or micro-structure on contacting material surfaces. First developed in 2012 [6], TENGs have attracted great interest of researchers in recent five years [7]–[11]. The high output voltage in broadband frequency for converting mechanical energy to electricity enables triboelectric energy harvesters applicable in various practical applications [12]–[16]. Instead of adding micro- and nano-structure, we prove the concept that macroscale surface structure using common low-cost materials can also achieve reasonable results.

In this paper, we first propose a novel self-powered solution for wearable motion sensing for human physical activity recognition. The new motion sensor provides a new perspective for boosting the battery life of wearable sensor nodes. The main contributions of this paper are summarized as follows.

1) We develop the first self-powered solution from the sensor itself for wearable motion sensing for human physical activity recognition for the application in WIoT.
2) We develop the detailed physical model, design method, fabrication and manufacturing process, and performance valuation for both self-powered motion sensing and

Manuscript received November 24, 2017; revised February 2, 2018 and March 12, 2018; accepted March 16, 2018. Date of publication March 21, 2018; date of current version January 16, 2019. This work was supported by the National Science Foundation under Grant 1710862. *(Corresponding authors: Shiyan Hu; Ye Sun.)*

H. Huang, X. Li, and S. Liu are with the Department of Mechanical Engineering and Engineering Mechanics, Michigan Technological University, Houghton, MI 49931 USA.

S. Hu is with the Department of Electrical and Computer Engineering, Michigan Technological University, Houghton, MI 49931 USA (e-mail: shiyan@mtu.edu).

Y. Sun is with the Department of Mechanical Engineering and Engineering Mechanics and the Department of Biomedical Engineering, Michigan Technological University, Houghton, MI 49931 USA (e-mail: yes@mtu.edu).

This paper is an extension of our previous conference publication, which can be found at http://ieeexplore.ieee.org/abstract/document/7591823/.

Digital Object Identifier 10.1109/JIOT.2018.2817841

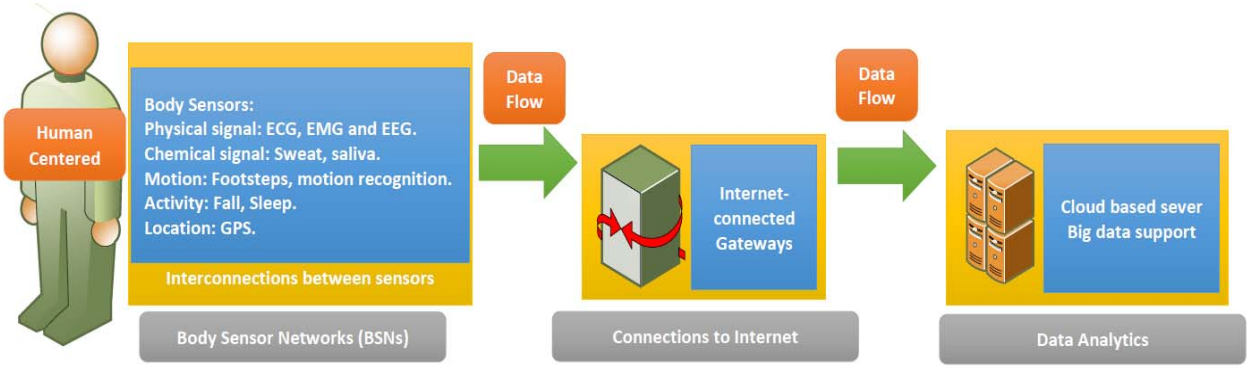

Fig. 1. General system architecture of WIoT.

energy harvesting in one device. Our triboelectric motion sensor can both achieve self-powered motion detection for physical activity recognition and energy harvesting.

3) We prove the concept that different from the existing TENGs, using only low-cost materials and manufacturing method without adding any nano- or micro-structure on the contacting surfaces can also provide reasonable output for practical applications, which may enable quick and low-cost mass production in industry.
4) Our experimental results demonstrate that our system can achieve similar comparable performance as the state of the art for the recognition of common physical activities including sitting and standing, walking, climbing upstairs and downstairs, and running with an average successful accuracy of over 80%. In addition, this triboelectric-based sensor can directly generate over 30-V peak-to-peak output voltage without any external signal conditioning circuits during random low-frequency motion (1–10 Hz), which enables energy harvesting simultaneously and reduces more than 25% energy consumption of the whole sensing hardware system.

This paper is organized as follows. Section II provides a brief review of WIoT on human physical activity recognition. Section III presents the overall system architecture of our proposed motion sensor in the front end of WIoT. Section IV illustrates the detailed physical model and design of triboelectric motion sensor and the theoretical analysis of energy harvesting. Section V describes the algorithms and validation experiments of activity recognition based on the self-powered motion sensor. Section VI describes the experimental validation of energy harvesting. A summary of the study is given in Section VII.

II. Literature Review

A. WIoT

Due to the emerging stage of WIoT, we first provide a brief overview to illustrate the concept. WIoT is a recently emerged concept of technological infrastructure that enables wearable body-worn or near-body sensors to communicate with each other and/or then connect to Internet access, which makes it viable for automating out-of-hospital healthcare with doctors in the loop, including remote diagnostic monitoring, treatments, and interoperability between customers and physicians [3]. A typical WIoT generally consists of wearable body sensor network (WBSN), interconnections with Internet for more services such as cloud computing and services, and further data analytics for decision support. Generally, WBSN is used as the sensing front end from human, which collects various data from human body directly for monitoring and therapeutic uses, or indirectly to sense human fitness, behavior, and rehabilitation [2].

In WIoT and its front end WBSN, a variety of vital signals can be acquired to provide data for long-term monitoring and disease diagnosis, especially for chronic conditions. A typical architecture of WIoT is shown in Fig. 1. In this paper, we focus on human activity recognition.

B. Human Physical Activity Recognition

Human physical activities are body movements related to skeletal muscles such as sitting, walking, stair climbing, falling, etc. The recognition of physical activities has extensive applications in health management, medical diagnosis and rehabilitation [17], [18], and has been considered as a valid approach for preventive, proactive treatment of cardiovascular diseases [19], diabetes [20], and obesity [21]. In addition, due to the increasing aging population worldwide, monitoring and assisting the activities of elderly people during their daily life has received considerable attention [22], [23]. Human physical activity recognition has much progress in recent decades, which can be generally classified into two categories, vision-based activity monitoring using single or multiple video cameras [24], [25] and inertial measurement units (IMUs) based on motion sensors such as accelerometers, gyroscopes, etc. These video-based systems can achieve high detection accuracy; however, they are limited to activities in certain areas such as well as the natural lighting conditions. Technical advances in recent years have made these sensors wearable and low cost. A number of studies using IMU-based physical activity monitoring have been proposed with new wearable system design [26] and robust and valid algorithms [27]–[30].

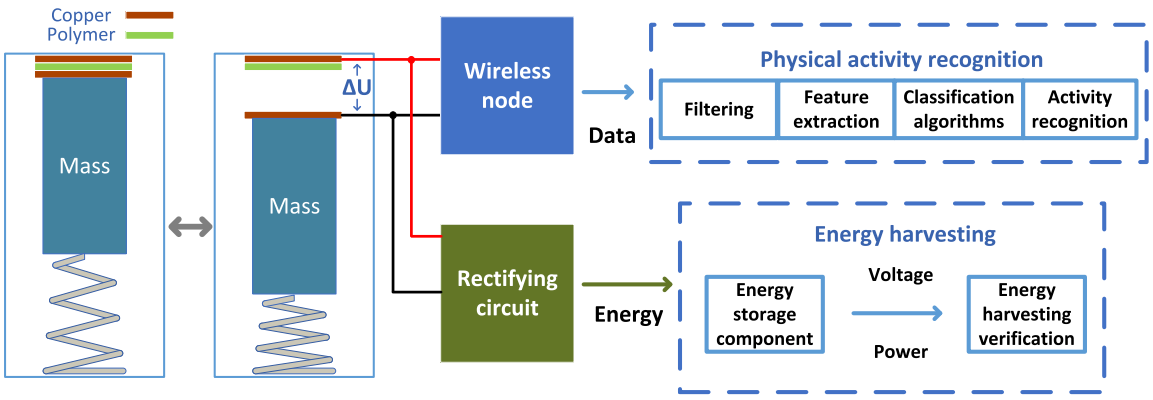

Fig. 2. System architecture.

C. Low Power Wearable Motion Sensors

For various WIoT, power supply is one of the major challenges for long-term monitoring, especially for aging population. Reducing power consumption of these wearable sensors and investigating power resources from ambient environment are two key issues for designing self-powered wearable devices, which has attracted much attention in recent years. Cohn *et al.* [31] successfully lowered the energy consumption of the wearables sensor down to 6.6 μW by developing an ultralow power motion detector to wake up the sensor node. Jafari and Lotfian [32] reduced at least three orders of the energy consumption of regular methods by their proposed low power architecture based on dynamic time warping. Although lots of studies have successfully decreased the power consumption of these IMU-based systems, the power issue still acts as a major concern in sustainability especially for long term monitoring. For these IMU-based motion sensors and systems, energy harvesting from motion is considered as a promising solution [4]. In our solution, both of the two key issues are considered for developing the self-powered and energy harvesting enabled wearable motion sensor system.

III. System Architecture

The wearable triboelectric motion sensor system consists of a triboelectric structure acting as both a self-powered motion sensor and an energy harvester and two corresponding subsystems for the two functions. Fig. 2 shows the sensor/energy harvester design and the overall system architecture. The left of the figure locates the proposed motion sensor, the output of which is connected with two subsystems. More detailed illustration about the motion sensor is presented in Section IV. The subsystem of the activity recognition consists of a wireless node for transmitting data and the physical activity recognition module for activity data collection and recognition. The other subsystem of motion energy harvesting includes the rectifying circuit for power conditioning and the energy harvesting verification module. The basic idea of the system design is to transform human motion to contact and separation sequence of the two active tribomaterial (i.e., triboelectric sensitive) layers, resulting in motion signals for activity recognition without power supply and energy harvesting verification. The design sketch of this motion sensor is shown in Fig. 3(b) and the detailed mechanism and model is illustrated in Section IV. The output signal of the motion sensor is captured by a 10-bit ADC and transmitted to the laptop wirelessly via the nRF24L01+ wireless node. The original high output of the structure is also stored by an energy storage component on board. The entire wireless sensor node is displayed in Fig. 3(a). The motion data are stored in the laptop for further analysis. In the physical activity recognition module, a lowpass filter is performed on the received data. After extracting the statistics features of the data, regular classification algorithms are developed for the recognition of patterns among various physical activities. More details about the procedure for the physical activity recognition is presented in Section V. The experiment results in Sections V and VI validate the feasibility of this new approach for physical activity recognition and the possibility to harvest energy from human motion using this kind of motion sensor.

IV. Triboelectric Motion Sensor and Harvester

Our new motion sensor design explores the new mechanism of triboelectrification for the conversion from mechanical motion to electricity, which enables to collect motion signals caused by human physical activities without any power supply as well as signal conditioning circuit. Compared to some low-power consumption motion sensors discussed in Section II, our sensor design lowers the energy consumption of the sensor down to 0. In addition, the high output voltage of this motion sensor is verified in Section VI to further perform energy harvesting from the motion. These advantages lead to excellent energy saving performance of our sensor design.

A. Sensor Design

To enable the conversion from mechanical vibration to electricity, three mechanisms are generally used in traditional accelerometers: 1) electrostatics using chargeable capacitor; 2) piezoelectricity based on piezoelectric materials; and 3) electromagnetics using motion of magnetic mass [33].

For these three mechanisms, the energy harvesting performances of them are significantly impacted by the frequency of mechanical vibration. Typically devices based on the three

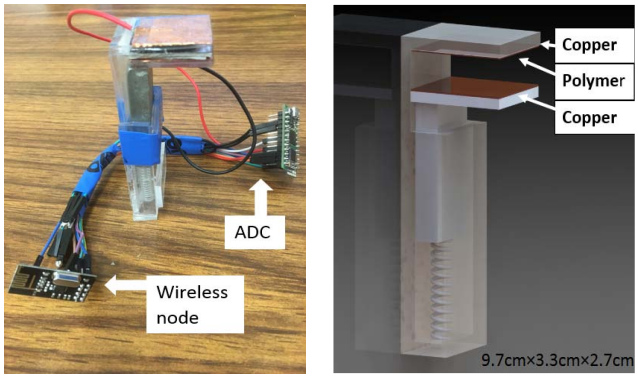

Fig. 3. Wireless triboelectric motion sensor node. (a) Photograph of the wireless sensor node. (b) Structure of the motion sensor.

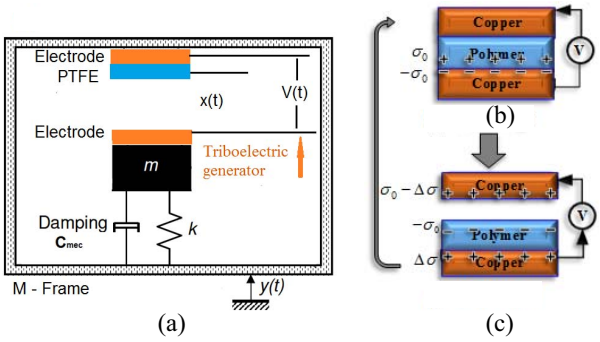

Fig. 4. Mechanism of the triboelectric motion sensor. (a) Motion measurement modeling. Triboelectric mechanism of (b) pressing and (c) releasing.

mechanisms resonate with a high Q-factor, which means that they have a narrow frequency bandwidth [34]. If the frequency of the mechanical vibration is away from the resonant frequency, the energy harvesting performance will drop significantly. This is a major challenge when considering harvesting energy from human motions which have wide-band and relatively low and random vibration frequency. Among the three commonly used methods, piezoelectricity-based method is the most widely used one. Though many existing studies [34]–[36] has significantly improved the Q-factor under certain situations with complex design and advanced materials, piezoelectricity-based methods achieve lower performance compared to our approach when handling the low and random frequency vibration source. In contrast, triboelectrification as an emerging mechanism is utilized in our design of the motion sensor to convert mechanical response to electric fluctuation due to its superior performance in wide-band and low frequency vibration. Commonly the surfaces of two materials contacting or sliding on each other will result in opposite charges on each surface. Subsequently, continuous contact-separation sequence will generate charge fluctuation which can be detected with electrodes.

In our design, the triboelectric motion sensor is composed of the substrates to support motion conversion, two active tribomaterial layers of size 3 $\times$ 2.5 cm^2 (i.e., copper and polytetrafluoroethylene (PTFE) thick film) for triboelectric generation, and two electrodes for charge collection as shown in Fig. 3(b). The substrates are used to form a mass-spring-damper system for dynamic motion conversion and generate continuous tribomaterial contact and separation. The output voltage is generated by contact-separation sequence of the two tribomaterial layers during motion. In the original position, the two active layers contact each other. There are charges accumulating on both surfaces with opposite sign, and the output voltage between the two electrodes is 0 V. When there is acceleration caused by motion, the mass with one tribomaterial layer will be separated due to stiffness of the spring, resulting in output voltage fluctuating as shown in Fig. 4(b) and (c).

Due to the fact that the distance between layers and the thickness of each layer are relatively small comparing with the contact area, the generated output voltage in the open circuit condition can be expressed as

$$V(t) = \frac{\sigma_0 x(t)}{\varepsilon_0} \tag{1}$$

where σ_0 is the surface charge density generated from triboelectricity caused by contact electrification of two active layers, $x(t)$ is the separation distance of copper and PTFE, and ε_0 is the vacuum permittivity. According to our previous experiments and other literature, the surface charge density can be estimated empirically, which is highly correlated to the contact materials and the contact condition, and the error of which is negligible compared to the motion signals.

In view of real system design, it is not feasible to anchor one part of the transducer to a fixed reference and the other to the vibration source in most cases [37]. This is why the principle of inertia is adopted to design the structure of the entire motion sensor. The substrates are designed to support the dynamic motion as shown in Fig. 3(b). The substrate of the motion sensor is composed of a frame, a movable mass connected with a spring, and a triboelectric generator. The dynamic motion conversion using this triboelectric structure is modeled as Fig. 4(a)–(c). The frame is attached to human body which is the vibration source during motion. The relative motion of the mass is controlled by the law of inertia. Subsequently, the system is made vibrate by means of suspending the movable mass to a spring forming a unified mass-spring-damper system as shown in Fig. 4(a). Equation (2) is to describe the mass-spring-damper system for motion conversion with the consideration of triboelectric energy conversion as follows:

$$m\ddot{x} + (c_{\text{mec}} + c_{\text{tribo}})\dot{x} + kx = -M\ddot{y} \tag{2}$$

where x represents the motion of the mass which is the separation distance of the two tribomaterial layers; $\ddot{x}$ and $\dot{x}$ are the second and first order derivative of x, respectively; y represents the frame movement; m is the movable mass and M denotes the mass of the frame; k is the coefficient of elasticity of the spring; and c_{mec} and c_{tribo} are the damping coefficients caused by parasitic effects and electricity conversion as some kinetic energy of the moving mass is converted into electrical energy whereas some is damped by parasitic effects of the mechanical system. With different types of motion input, the generated relative distance between the upper and lower substrates can be

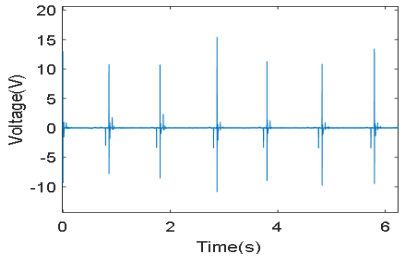

Fig. 5. Waveform of test signal.

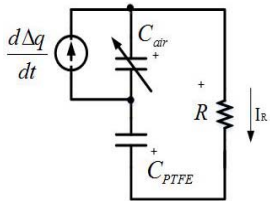

Fig. 6. Equivalent circuit model of triboelectric motion energy harvester.

acquired by solving (2). In our experiment, there are two types of motion scenarios, the free vibration with damped vibration ended in a relatively longer time and the forced vibration with periodic motion input during fast movement. The analytical solution to the free vibration with the substrate attached to the table for experimental validation can be expressed as

$$x(t) = X_0 e^{-\xi\omega_n t}\cos\left(\sqrt{1-\xi^2}\omega_n t - \phi\right) \tag{3}$$

where $x(t)$ is the displacement of the mass relative to its equilibrium position; $\xi = (c_{\text{tribo}} + c_{\text{mec}})/2\sqrt{mk}$ and $\omega_n = \sqrt{(k/m)}$ are the damping ratio and the natural frequency; and ϕ is the phase shift. When the relative distance $x(t)$ fully follows the continuous motion input $y(t) = Y_0 e^{j\omega t}$, the analytical solution without considering the coupled term is [38]

$$x(t) = \frac{\omega^2}{\omega_n^2 - \omega^2 + 2j\xi\omega_n\omega} Y_0 e^{j\omega t}. \tag{4}$$

During one motion cycle, the distance between the two active tribomaterial layers is changing from full separation with maximum distance, to close enough when finally they will touch each other as shown in Fig. 4(b) and (c). The motion cycle repeats with human motion and the output of the voltage is fluctuating with the distance change. Subsequently, the generated voltage can be calculated via (1), (3), and (4), which is highly correlated to human motion theoretically. The motion sensor is then validated by applying a low-frequency, equally controlled, periodic motion (∼1 Hz), and the generated output signal is shown in Fig. 5. The reciprocating waveform demonstrates that the motion sensor has eligible stability and sensitivity for sensing motions and the feasibility for designing a self-powered motion sensor. The peak-to-peak voltage is around 20 V, which also enables energy harvesting even in low frequency range. Based on the mechanism of motion conversion and triboelectrification, the new sensor can generate signal patterns during different activities for activity recognition without power supply.

B. Theoretical Analysis of Energy Harvesting

In order to further explore how to harvest motion energy under low frequency, we then conducted the theoretical analysis of using the triboelectric motion sensor for power generation as a motion energy harvester. In this section, we discuss the theoretical modeling and further validate it in Section VI. As shown in Fig. 4, the two tribomaterials are forced to get into contact and separate with each other by the mechanical movement. Subsequently opposite static charges are then distributed on the contact surfaces of the two tribomaterial layers because of triboelectrification. In one contact-separation cycle, these induced charges are generally assumed to be uniformly distributed on the surfaces of the dielectric tribomaterials with the charge density of σ_0. According to the Gauss's law, this charge generation will result in a surface potential, $V_s = \sigma_0 d_0/\varepsilon_0\varepsilon_r$, with the bottom electrode connecting to the ground [39], where ε_0 is the vacuum permittivity, ε_r is the relative permittivity of PTFE, and d_0 is the thickness of the PTFE layer. In the equivalent circuit model, this surface potential then acts as a voltage source [40]. In addition, as the area of the two active material layers, S, is much greater than the distance x between them, the triboelectric structure can be modeled as parallel plate capacitors as shown in Fig. 6.

When connecting to external loads, the charges are then transferred and the generated electrical energy can be used by the load or stored in an energy storage component such as a larger capacitor. The triboelectric induced charge, $q_0 = \sigma_0 S$, and the relative movement of the two substrates of the triboelectric structure, $x(t)$, cause charges redistribution on the two electrodes with a current through the load. According to Fig. 4, we propose a new equivalent circuit model as shown in Fig. 6 shows the equivalent circuit model of the triboelectric structure with a load resistor R. In one contact-separation cycle, the physical model is actually similar to an electrostatic harvester with precharged electret in between as charge source. In previous models, this harvester is generally modeled as a voltage source in series to a changeable capacitor caused by input motion. The changeable capacitor is composed of two or more capacitors in series due to the different dielectric materials between the electrodes. The changing distance between the upper and lower part of the energy harvester acts as one changing capacitor with air in between.

Actually, due to the emerging stage of triboelectric generators, the equivalent circuit model may still be debating. In this paper, instead, we propose a new model by adding a current source, $d\Delta q/dt$, in parallel to the changing air layer. This is because when capacitors are connected in series, each of them stores instantaneous charge equal to each other. However, this may not be the case for both air layer and polymer layer. Assuming that charge amounts through the air layer C_{air} and the polymer layer C_{PTFE} are q_1 and q_2, respectively, then according to Gauss's law, we have $q_0 = q_2 + q_1$. The transferred charge amount is then $\Delta q = q_2 - q_1 = \Delta\sigma(t)S$. In our proposed equivalent circuit model as Fig. 6, according to Kirchhoff's law with the sign marked

$$R\frac{dq_2}{dt} = u_{C_{\text{air}}} - u_{C_{\text{PTFE}}} \tag{5}$$

where $u_{C_{\text{air}}} = q_1(t)/C_{\text{air}}(x)$ is the voltage through the air layer capacitor, $C_{\text{air}}(x) = \varepsilon_0 S/x(t)$, which is changed by the relative motion of the upper and lower part, where $x(t)$ can be calculated by (3) and (4) in those two motion conditions; $U_{C_{\text{PTFE}}} = q_2(t)/C_{\text{PTFE}}$ is the voltage through the polymer layer, $C_{\text{PTFE}} = \varepsilon_0\varepsilon_r S/d_0$. Replacing these terms into (5) and replacing q_1 with $q_0 - q_2$, we have

$$R\frac{dq_2}{dt} = -\frac{q_2}{S\varepsilon_0}\left(\frac{d_0}{\varepsilon_r} + x(t)\right) + \frac{\sigma_0 x(t)}{\varepsilon_0}. \tag{6}$$

This result is the same as [8] which uses the analysis of electric field and Gauss's law without establishing the equivalent circuit model. By solving (6), we are able to solve for the analytic solution of $q_2(t)$, which can be expressed as

$$q_2(t) = \int_0^t \frac{\sigma_0 x(\tau)}{R\varepsilon_0} e^{\int_0^\tau \frac{\frac{d_0}{\varepsilon_r}+x(\tau)}{RS\varepsilon_0}d\tau}\, e^{-\int_0^t \frac{\frac{d_0}{\varepsilon_r}+x(\tau)}{RS\varepsilon_0}d\tau}. \tag{7}$$

Therefore, the expression of the output voltage through the load resistor is

$$u_R(t) = \frac{\sigma_0 x(t)}{\varepsilon_0} - \frac{\frac{d_0}{\varepsilon_r} + x(t)}{S\varepsilon_0} e^{-\int_0^t \frac{\frac{d_0}{\varepsilon_r}+x(\tau)}{RS\varepsilon_0}d\tau} \times \int_0^t \frac{\sigma_0 x(\tau)}{R\varepsilon_0} e^{\int_0^\tau \frac{\frac{d_0}{\varepsilon_r}+x(z)}{RS\varepsilon_0}d\tau}. \tag{8}$$

According to (7) and (8), the parameters such as triboelectric charge surface density, area of the contact surface, and the velocity of electrode can be determined empirically according to experimental condition, and the output voltage can then be calculated using (7) and (8). Then the generated power can be estimated by

$$P_{\text{out}}(t) = \frac{u_R^2(t)}{R}. \tag{9}$$

The average power can be estimated by

$$P_{\text{avg}} = \frac{1}{t_j - t_i}\int_{t_i}^{t_j} P_{\text{out}}(t)dt. \tag{10}$$

In the experiment, we validate this model by comparing the experimentally measured voltage and theoretically calculated voltage of different load resistors, which has not been conducted in the current literature yet. This equivalent circuit model for triboelectric energy harvesters may provide a new solution for fundamental circuit modeling with triboelectric energy harvester.

C. Energy Saving Performance

For a typical accelerometer-based wearable motion sensor system, the power consumption of the accelerometer is normally around 1 mW, and the commonly used microcontroller consumes nearly 3 mW (e.g., MSP430 consumes about 3 mW in active mode) with the circuitry about 9 μW [32]. Therefore, the total power consumption for the sensing hardware is 4.009 mW. With our proposed self-powered motion sensor except for the energy savings from its energy harvesting function, the sensing hardware power consumption will be lowered to $4.009 - 1 = 3.009$ mW, which saves almost 25% of the total power consumption for the sensing hardware. Table I compares the sensing hardware power consumption of the IMU-based low power wearable sensors with that of our proposed sensor.

TABLE I
SENSING HARDWARE POWER CONSUMPTION

Methods	[41]	[42]	[32]	Proposed
Power consumption (mW)	18	5.2	4.25	3

V. EXPERIMENTAL RESULTS ON ACTIVITY RECOGNITION

Human physical activity recognition has become a highly attractive task for many applications, not only in the field of human-centered healthcare but also in developing advanced human-machine interfaces because of the valuable information including various biomechanical and physiological parameters of human physical activities. In human-centered healthcare, human physical activity plays an important role in the therapy of mobility reducing disorders such as chronic pulmonary disease, obesity, stroke, and so on [17]. For example, in chronic pulmonary disease, pulmonary rehabilitation requires general exercise to improve physical functioning and quality of life, which is typically performed with in-hospital programs for improvements in the ability to carry out daily physical activity such as periods of extended walking. With the wearable physical activity recognition technology such as the one proposed in this paper, the pulmonary rehabilitation can be achieved through low-cost out-of-hospital healthcare, and the life quality of the patients can be greatly improved. In the field of human-machine interface, human physical activity is able to provide the useful source of contextual knowledge for developing more complex and abundant human-machine interactions [28]. For example, in some movement supporting systems for motor-impaired people and elderly, physical interaction can be designed for the smart recognition of human physical activities as well as detecting fall.

In this paper, the wireless triboelectric motion sensor is placed on the upper part of the calf to collect the motion data generated by different activities. Experiments are conducted to collect specific motion data for walking, sitting and standing, climbing stairs, and running. The patterns of the data originated from these different activities are recognized by classification algorithms.

A. Experiment

In the experiments, the application for human physical activity recognition is validated. For the recognition objective, we choose the common activities including sitting and standing, walking, climbing upstairs, downstairs, and running for activity recognition. To demonstrate the functionality of physical activity recognition, a classic classification problem will be solved in the following parts. The most popular classification methods, namely support vector machine (SVM) and logistic regression (LR), are used to illustrate the effectiveness of our sensor design. Although other classification methods such as k-nearest neighbors, neural network can also be used, according to our experience, the performances of these methods are similar.

B. Activity Recognition

In the experiment, people wear the wireless sensor node as Fig. 7 shows, and perform actions as instructed.

Fig. 7. Sensor position in the experiment.

TABLE II
RECOGNITION ACCURACY USING SVM

Activities	Description of activities	Duration
a	Sitting and standing	5 times
b	Walking	10 steps
c	Climbing stair up	6 steps
d	Climbing stair down	6 steps
e	Running	10 steps
f	Continuous activities including the above activities	Random

A time-synchronized video recording is used for calibration. Five groups of tests consist of the dataset and three subjects are involved in each group of the test. For each subject, after the sensor node is placed properly, the subject is required to perform the group of activities in Table II.

After data acquisition, a necessary procedure is used to determine the training data for the recognition algorithm. As the great difference of the subjects motion patterns, such as different walking or running speed, each subject should be considered individually. First, the patterns of different activities are extracted manually for each subject to be used as the training data for recognition from activities *a–e* in Table II. Intuitively the element of these activities is one step, so the waveforms of one-step of these actions are extracted manually for training samples. For the sitting and standing action, one sitting and standing action counts an element. Take walking as an example. According to the video, the waveform of each step can be located by the time period that each step lasts. For a simple implementation of the further recognition algorithm, the time period of one-step of walking is constant, which is the mean time periods of one-step of walking. Fig. 8 shows the waveform of one-step of different actions and Fig. 9 shows the typical waveform of walking and running as examples. It has been discussed that the statistical metric is popularly used in physical activity recognition with small computational cost and minimal memory requirements [43]. The statistic parameters are used as the features of training data including the mean, variance, max, min value and root mean square (RMS) of the training sample. For example, one-step of walking is extracted as the training dataset. The mean M, variance V, max value Max, min value Min, and RMS of the one-step walking are chosen to be its features. In order to demonstrate the performance of this sensor in physical activity recognition, two standard classification algorithms are used for the physical activity pattern recognition in this experiment.

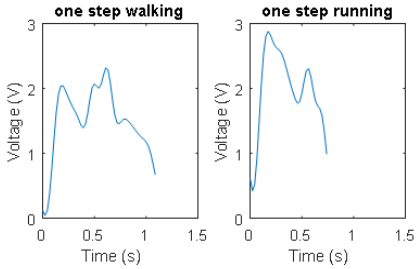

Fig. 8. Waveforms of one step of walking and running sample.

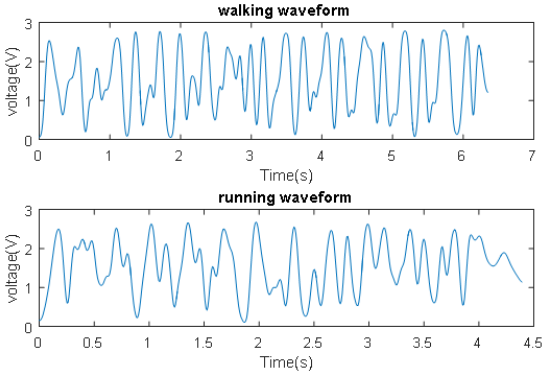

Fig. 9. Waveforms of walking and running.

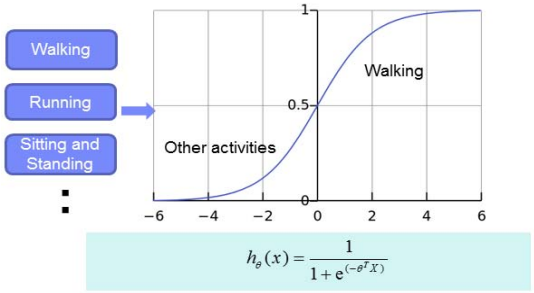

Fig. 10. LR model for activity classification.

C. Physical Activity Recognition Algorithm

1) Logistic Regression: LR is a statistic regression method for classification based on probability, which is able to map a set of explanatory variables x_i, that can be discrete and/or continuous, to binary response variable $y_i \in \{0, 1\}$, as illustrated in Fig. 10. This is performed by estimating the probability using the function of the form [44]

$$P(y = 1|X) = h_\theta(X) = \frac{1}{1 + e^{(-\theta^T X)}} \tag{11}$$

where y is the binary response variable, X is the explanatory variable, and θ is the coefficient vector determined from training process. In the training process, the classifier is constructed by determining the value of θ to make that the probability $P(y = 1|x) = h_\theta(x)$ is large when x belongs to the class of $y = 1$ and small when x belongs to the class of $y = 0$. For a given set of training sample with binary labels, the value of θ can be calculated by solving the optimization problem of

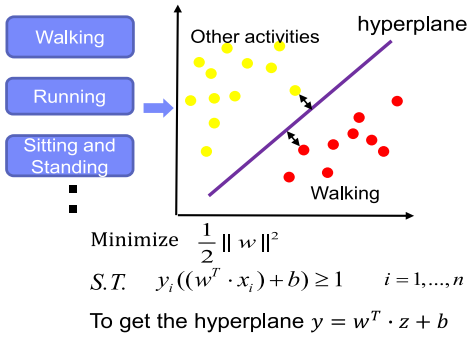

Fig. 11. SVM for activity classification.

minimizing the following equation [44]:

$$J(\theta) = -\sum_i (y_i \log(h_\theta(x_i)) + (1-y_i)\log(1-h_\theta(x_i))). \quad (12)$$

After the determination for θ, the classification can be performed by checking whether the classifier

$$h_\theta(x) = \frac{1}{1+e^{(-\theta^T X)}} > 0.5. \quad (13)$$

2) SVM Algorithm: The method of SVM is widely involved in many research areas and proved to be an effective way to perform classification used to recognize the pattern of activities [45]. The SVM separates data using linear decision hyperplanes. If the data cannot be separated linearly, SVM utilizes a kernel function to transform the data into a new vector space so that the data can be linearly separated. The SVM approach constructs a hyperplane or set of hyperplanes in this new high- or infinite-dimensional space, which can be used for classification, regression, or other tasks. Intuitively, a good separation is achieved by the hyperplane that has the largest distance to the nearest training-data point of any class (so-called functional margin), since in general the larger the margin the lower the generalization error of the classifier.

Here one step walking sample is used as the positive training data $[p_i, 1]$, in which 1 represents the walking group, and other activities including sitting up and down, running and climbing stair are used as negative training data $[n_j, 1]$, 0 represents the nonwalking group. Thus, the training data can be expressed by

$$T = \{[p_i, 1], [n_j, 0]\}, \quad i = 1, 2, \ldots, 5; j = 1, 2, \ldots, N. \quad (14)$$

The next step is to map these training data to a higher dimension space so that we can find a maximum-margin hyperplane that divides the walking group and other activities group, which is called the SVM classifier. In this paper, a quadratic kernel function is selected to transform the data to a new vector space. Finally, new test samples, z_i, can be classified by the hyperplane as shown in Fig. 11.

The procedure of implementing the two algorithms for physical activity recognition is similar. Take walking for example, the main steps are performed as follows.

1) *Preprocess the Original Signal:* Using the low-pass filter to remove the high frequency components, as the walking frequency is generally lower than 10 Hz.

TABLE III
RECOGNITION ACCURACY USING LR

Continuous activities No.	Recog. sitting standing	Recog. walking	Recog. upstair	Recog. downstair	Recog. running
#1	95.4%	87.0%	86.0%	76.7%	97.7%
#2	71.2%	83.6%	77.5%	69.3%	85.1%
#3	81.8%	74.4%	90.9%	78.1%	89.1%
#4	83.3%	75.9%	88.8%	77.7%	89.7%
#5	62.7%	75.4%	38.6%	43.2%	83.7%
Average	81.4%	80.2%	72.5%	65.5%	84.6%

TABLE IV
RECOGNITION ACCURACY USING SVM

Continuous activities No.	Recog. sitting standing	Recog. walking	Recog. upstair	Recog. downstair	Recog. running
#1	91.7%	75.0%	54.8%	66.7%	95.2%
#2	76.2%	78.6%	69.0%	71.4%	92.8%
#3	88.2%	87.3%	92.7%	85.5%	90.9%
#4	85.4%	80.3%	72.2%	74.5%	93.0%
#5	62.7%	83.6%	76.5%	74.1%	93.1%
Average	80.8%	81.0%	73.0%	74.4%	93.0%

2) *Extract the One Step of Actions As Training Data Manually and Compute the Five Features:* Mean, variance, max, min, and RMS. According to the methods described above, a formula of the classifier is constructed. Then search in the sample data, $S(x_1, x_2, \ldots, x_n)$ by scanning with a window of the same length of the training data and computing the features.
3) Calculate (11) and the hyperplane for the test samples to determine if the sample is a walking action.

All the activity recognition follows the above steps. Fig. 12 shows the sitting, walking and running period recognized during a period of continuous activities of two subjects. The ratio between correct recognition periods and real activity periods is selected to indicate the recognition accuracy. The correct recognition periods include the correct target activity and nontarget activity periods. They are also called true positive and true negative. On the contrary, the false detection can be defined as the ratio between false recognition periods and the real activity periods. The false recognition periods including the false target activity and nontarget activity periods as false positive and false negative. The final results of both algorithms are listed in Tables III and IV. From Tables III and IV, the recognition accuracy of over 80% can be achieved for walking, sitting, and standing. However, that of climbing upstairs and downstairs is relatively low, which needs further investigation.

To improve the recognition accuracy, the proper training samples of activities according to the features should be selected carefully. As the objective is to recognize the time period of activities, the length of training sample can be optimized to maximize the recognition accuracy. According to our experiment, the length of activity affects the feature to the extent that a longer training sample has better performance in the recognition. Fig. 13 shows the different training samples of walking. Though the one step of walking sample is quite similar, there are still some strayed waveforms that diversify the one step of walking samples. Considering the three step

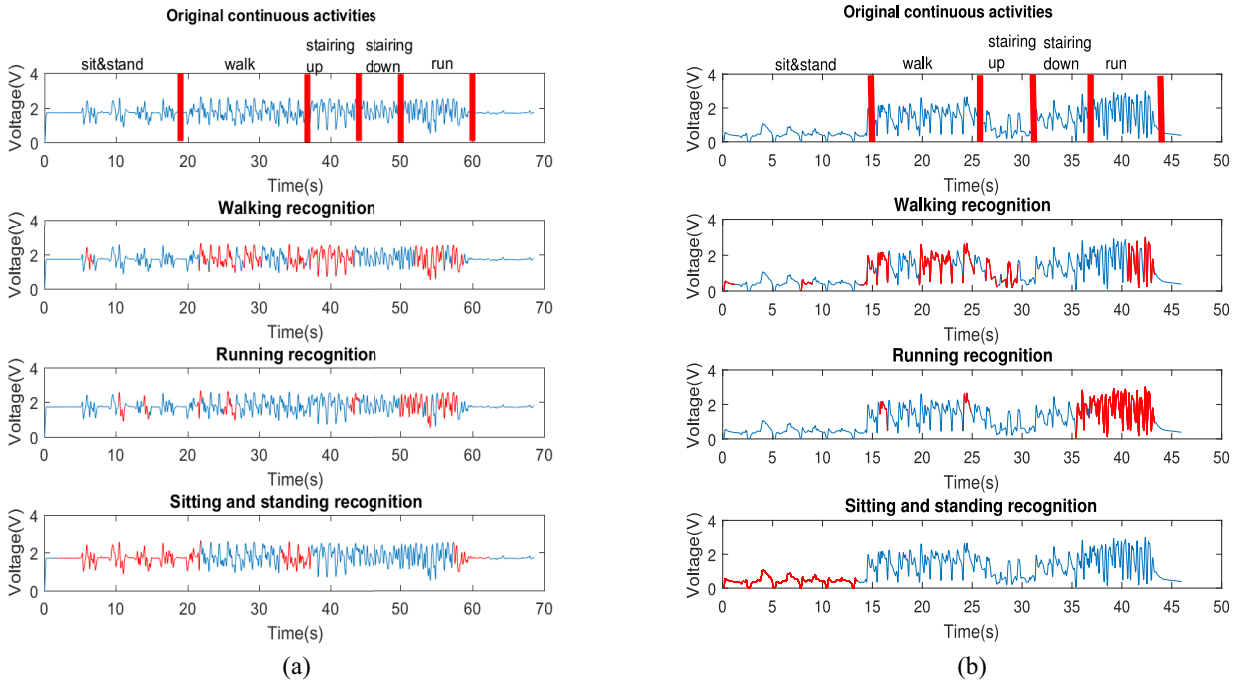

Fig. 12. Recognition results of (a) subject 1 and (b) subject 2. In both figures, the first figure is the original continuous activities and the second figure shows the recognized walking in red, the same as other two figures.

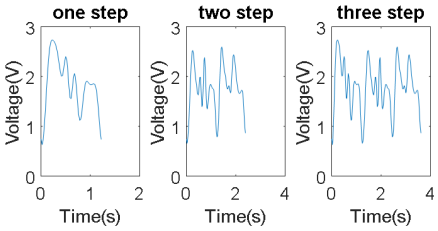

Fig. 13. Waveforms of walking samples.

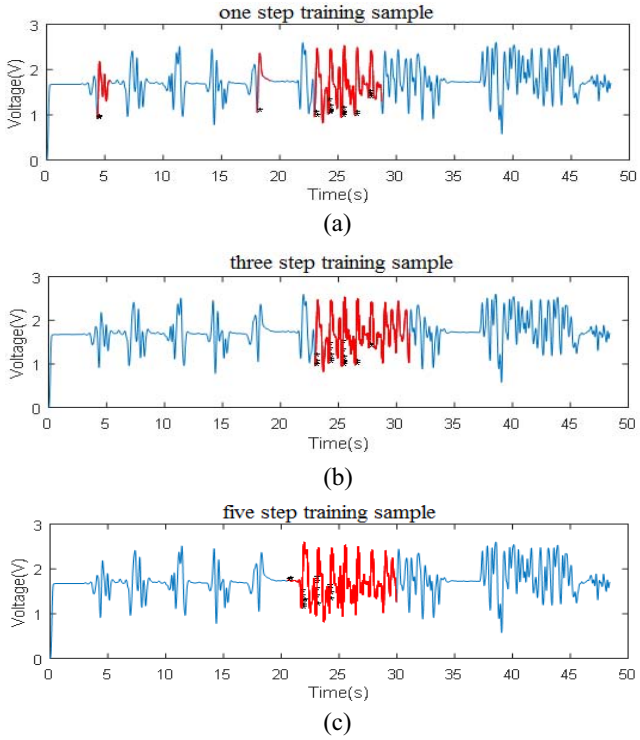

Fig. 14. Red part is recognized walking using (a) one step walking sample, (b) three step walking sample, and (c) five step walking sample.

training sample, it seems that the difference of single step waveform makes it better capability of fault tolerance. To verify the idea, different length of training samples are chosen for the recognition. Fig. 14 presents the result of different length of training samples. There are three parts of the whole activity. The first part contains five sitting up and down actions, and the second part is ten steps of continuous walking, and the third part is ten steps of continuous running. It can be shown that one step training sample has lower recognition accuracy, and the three and five step training samples have a close recognition accuracy. In this way, the proper training sample can be obtained to maximize the recognition accuracy. On the other hand, this training sample can hardly recognize one or two steps of walking, which means the recognition precision is lower. This tradeoff depends on the objective of specific recognition tasks which is out of the scope of this paper.

For human physical activity recognition, the recognition accuracy is still a big challenge, especially in some rehabilitation therapy program which requires strict activity recognition, as some activities may have similar patterns of motion signals such as climbing upstair and downstair. The above discussion is one of the options for improving the activity recognition accuracy. In fact, there still exists many options to work out. For example, more advanced feature may be extracted from the motion signal of the activities as well as well-designed algorithms can be performed

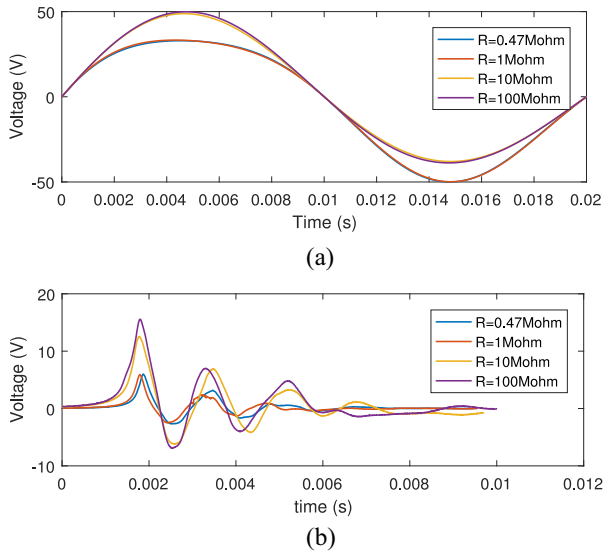

Fig. 15. Influence of resistance load on the performance of energy harvesting. (a) Theoretically calculated voltage curve of different resistors. (b) Experimental results of voltage curve of one time motion.

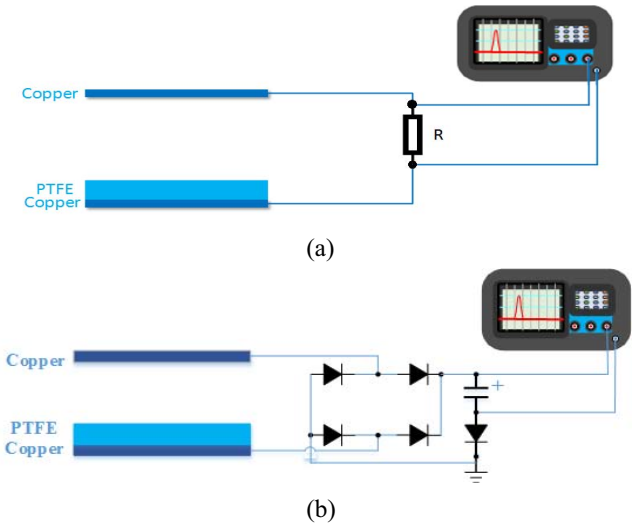

Fig. 16. Energy harvesting subsystem testing architecture. (a) Connecting with resistors. (b) Charging capacitors.

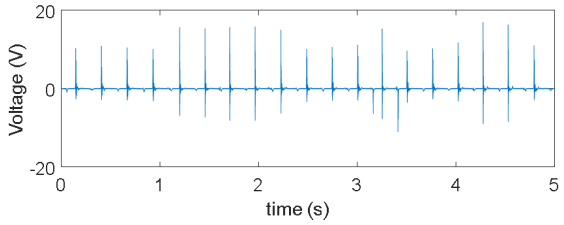

Fig. 17. Voltage of the load resistor during motion-induced contact and separation.

to better classify different activities. These can be our future works.

VI. Experimental Results on Energy Harvesting

Our motion sensor can achieve high output voltage under low and random frequency based on triboelectrification, demonstrating the feasibility to work as an energy harvester. Thus, we also investigate the energy harvesting performance of this ultralow-cost triboelectric structure with simulation and experiment.

A. Sensor Output Simulation and Experiment

The simulation is based on the theoretical analysis in Section IV for the voltage between the two electrodes with and without load resistors. An experiment for evaluating the performance of energy harvesting was also conducted to validate our theoretical analysis. For the theoretical analysis, the voltage curve of one cycle, which is the process starts from contact to separate until the distance between electrodes arrives $x_{\max}$, is calculated by estimation of constant parameters. According to (8), the voltage curve can be plotted as Fig. 15(a) by specifying the parameters estimated below.

1) Maximum separation distance: 0.003 m.
2) Thickness of PTFE: 200 μm.
3) Area size of the contact surface: 7.5 cm^2.
4) Triboelectric charge surface density: 10 μC/m^2.
5) Average velocity, v: 0.1 m/s.

Different resistors are used to investigate how the voltage varies when the two layers contact and separate. Fig. 15(a) shows the simulation results, from which it can be noticed that the maximum voltage it can achieve goes up when the value of load resistors goes up. The time of the process of the voltage variance is at the millisecond level which appears as a sharp peak from the normal voltage curve. In addition, the time interval of one cycle of the process will increase with the value of the resistor increases. In the experiment, the sensor is controlled to make the two layers contact and separate at a certain speed so that the signals can maintain a relatively stable frequency at 5 Hz. Different values of resistors are tested by connecting individually between the two electrodes of the triboelectric structure as shown in Fig. 16(a). The voltage of the resistor is measured by a digital oscilloscope. Fig. 17 shows the instantaneous voltage waveform generated by contact-separation sequence of the two tribomaterial layers in the triboelectric structure without load resistor or capacitor. Fig. 15(b) indicates the different load curves of a one-time motion. The average power calculated in a one-time motion can be up to 3 μW.

B. Energy Harvesting Experimental Validation

The experimental results show that the generated output voltage align with the envelope of calculated results in which the voltage of the load resistor, u_R, shows a damped sinusoid waveform. This waveform does not change much with load resistance, whereas it is dominated by the input motion frequency, which aligns with our proposed model. The damping of the sinusoid waveform is theoretically caused by the damping resulting from mechanical parasite effects and energy conversion as illustrated in (2) and the damping of surface charge density caused by triboelectricity. In the simulation,

TABLE V
PARAMETERS WHEN CHARGING CAPACITORS

Capacitors (μF)	Max voltage (V)	Time for charging to max voltage (sec)	Max peak power (μW)
2.2	0.53	16.5	9.4
4.7	0.43	29.7	7.1
10	0.41	51.2	7.0

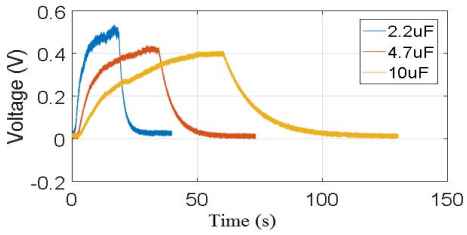

Fig. 18. Voltage of charging different capacitors.

we did not consider the damping of surface charge density. The difference can come from the following reasons.

1) In the theoretical analysis, the surface charge density is assumed to be a constant. This is because of the relatively stability of PTFE. However, as we use copper as another active tribomaterial, the generated surface charge density, σ_0, is probably follows $\sigma(t) = \sigma_0 e^{(-t/\tau)}$. In the real experiment, the generated charge distribution may further be influenced by surface condition, environment, and external load, which could be small and changeable.
2) In the real movement, the distance between the two tribomaterial layers $x(t)$ is not ideal as the theoretical calculation, as the spring constant in the experiment can be higher than the experimentally measured one during random motion. Therefore, the nature frequency of the motion structure which finally dominates the frequency of the voltage of the load resistor is actually higher in the experiment, which will cause signal envelop mismatching.
3) Due to our sensor design for activity recognition, the maximum separation distance is not high which also cause lower output voltage.

In order to harvest the motion induced energy, we add a power conditioning circuit which is based on a bridge rectifier circuit and an energy storage component which are different capacitors for calibration. Three capacitors of 2.2, 4.7, and 10 μF were selected to investigate the harvesting performance. Fig. 16(b) shows the energy harvesting testing architecture. The oscilloscope is to measure the capacitor voltage which indicates the harvested energy. Also, the input motion is controlled at approximately 5 Hz. The triboelectric structure is forced to vibrate under 5 Hz to charge the capacitor. Fig. 18 presents the results of charging different capacitors. The 2.2-μF capacitor can be charged fast until reaching the maximum voltage which is 0.53 V in 16.5 s. Then the input motion stopped the capacitor to discharge. The maximum peak power can be achieved is up to 9.4 μW for the 2.2-μF capacitor; however, the discharging is also fast. Table V shows the results of the energy harvesting performance when charging capacitors. It can be noticed that the sensor can provide continuous voltage for the capacitor when the motion continues, which means it is able to harvest energy from the motions. The amount of the harvested energy can be up to the same amount of consumed energy by the circuitry of the sensing hardware as mentioned in Section IV.

One might wonder whether the performance can be further improved. There are two possible ways that can be considered. The first is to increase the contact surface area by decorating the contact surfaces with structures such as pectination. The second way is to change the contact materials to other more triboelectric sensitive materials. Both of the two methods can increase the generated voltage level by the triboelectric structure which can be our future work. In addition, energy saving performance can also be improved via other methods. As wireless transmission is one of the basic aspects of the WIoT technology, which consumes most of the energy supply of wireless wearable devices, reducing the amount of signal transmission is also considered as a promising method. This is also our future work.

VII. CONCLUSION

In this paper, we develop the first self-powered solution of wearable sensor system for physical activity recognition based on triboelectrification other than the traditional motion sensors. We demonstrate the dual functionality of the proposed wireless system of physical activity recognition and energy harvesting using the same triboelectric structure. For activity recognition, the signal conditioning circuit of the analog signal is not needed for this new design. Regular methods including SVM and LR are used for pattern recognition. The successful accuracy can reach up to 90% for certain activity, which showed the similar comparable performance to the state of the art. The energy harvesting performance was validated by charging different load resistors and capacitors under low frequency motion. The power consumption of the sensing hardware is estimated and compared with similar IMU-based low power wearable sensor systems, which saves at least 25% of the power of regular sensing hardware. This system demonstrates the feasibility of providing new solutions considering energy consumption and enable physical activity monitoring using WIoT in daily life at very low cost.

Further, theoretical and practical contributions can be summarized. For the theoretical contribution, we design the first triboelectric structure coupling with a damping system for sensing and recognizing human motion and harvesting energy from human motion at the same time using triboelectrification mechanism. We theoretically analyze and verify how human motion is detected and transferred to output signals. In addition, we develop the equivalent circuit model for understanding how mechanical energy in human motion can be harvested by using our design. For the practical contribution, according to our theoretical analysis, we develop the first self-powered solution of wearable sensor system for human physical activity recognition. The recognition rate of the physical activity

of our system is comparable to the state of the art, while the energy saving functionality saves at least 25% of the power of regular sensing hardware. Our newly proposed method not only develops a feasible application for performing task of human physical activity recognition using WIoT technology with self-powered motion sensor devices, but also provides a new perspective for solving the problem of the power limit of WIoT in future studies. As WIoT is playing an increasingly important role on various human-centered applications, this new perspective will bring in a promising foundation for constructing the next generation self-powered WIoT by facilitating various wearable applications.

REFERENCES

[1] C. S. Kruse, M. Mileski, and J. Moreno, "Mobile health solutions for the aging population: A systematic narrative analysis," *J. Telemed. Telecare*, vol. 23, no. 4, pp. 439–451, 2017.

[2] C. C. Y. Poon, Q. Liu, H. Gao, W.-H. Lin, and Y.-T. Zhang, "Wearable intelligent systems for e-health," *J. Comput. Sci. Eng.*, vol. 5, no. 3, pp. 246–256, 2011.

[3] S. Hiremath, G. Yang, and K. Mankodiya, "Wearable Internet of Things: Concept, architectural components and promises for person-centered healthcare," in *Proc. IEEE EAI 4th Int. Conf. Wireless Mobile Commun. Healthcare (Mobihealth)*, Athens, Greece, 2014, pp. 304–307.

[4] P. D. Mitcheson, E. M. Yeatman, G. K. Rao, A. S. Holmes, and T. C. Green, "Energy harvesting from human and machine motion for wireless electronic devices," *Proc. IEEE*, vol. 96, no. 9, pp. 1457–1486, Sep. 2008.

[5] P. L. Green, E. Papatheou, and N. D. Sims, "Energy harvesting from human motion and bridge vibrations: An evaluation of current nonlinear energy harvesting solutions," *J. Intell. Mater. Syst. Struct.*, vol. 24, no. 12, pp. 1494–1505, 2013.

[6] F.-R. Fan, Z.-Q. Tian, and Z. L. Wang, "Flexible triboelectric generator," *Nano Energy*, vol. 1, no. 2, pp. 328–334, 2012.

[7] S. Niu *et al.*, "Theory of sliding-mode triboelectric nanogenerators," *Adv. Mater.*, vol. 25, no. 43, pp. 6184–6193, 2013.

[8] S. Niu *et al.*, "Theoretical study of contact-mode triboelectric nanogenerators as an effective power source," *Energy Environ. Sci.*, vol. 6, no. 12, pp. 3576–3583, 2013.

[9] S. Niu and Z. L. Wang, "Theoretical systems of triboelectric nanogenerators," *Nano Energy*, vol. 14, pp. 161–192, May 2015.

[10] S. Wang, L. Lin, and Z. L. Wang, "Nanoscale triboelectric-effect-enabled energy conversion for sustainably powering portable electronics," *Nano Lett.*, vol. 12, no. 12, pp. 6339–6346, 2012.

[11] Z. L. Wang, "Triboelectric nanogenerators as new energy technology and self-powered sensors—Principles, problems and perspectives," *Faraday Discussions*, vol. 176, pp. 447–458, Nov. 2014.

[12] W. Tang, C. B. Han, C. Zhang, and Z. L. Wang, "Cover-sheet-based nanogenerator for charging mobile electronics using low-frequency body motion/vibration," *Nano Energy*, vol. 9, pp. 121–127, Oct. 2014.

[13] C. Han, C. Zhang, W. Tang, X. Li, and Z. L. Wang, "High power triboelectric nanogenerator based on printed circuit board (PCB) technology," *Nano Res.*, vol. 8, no. 3, pp. 722–730, 2015.

[14] F.-R. Fan *et al.*, "Transparent triboelectric nanogenerators and self-powered pressure sensors based on micropatterned plastic films," *Nano Lett.*, vol. 12, no. 6, pp. 3109–3114, 2012.

[15] Q. Jing, Y. Xie, G. Zhu, R. P. S. Han, and Z. L. Wang, "Self-powered thin-film motion vector sensor," *Nat. Commun.*, vol. 6, p. 8031, Aug. 2015.

[16] Y. K. Pang *et al.*, "Triboelectric nanogenerators as a self-powered 3D acceleration sensor," *ACS Appl. Mater. Interfaces*, vol. 7, no. 34, pp. 19076–19082, 2015.

[17] A. Godfrey, R. Conway, D. Meagher, and G. ÓLaighin, "Direct measurement of human movement by accelerometry," *Med. Eng. Phys.*, vol. 30, no. 10, pp. 1364–1386, 2008.

[18] C.-C. Yang and Y.-L. Hsu, "A review of accelerometry-based wearable motion detectors for physical activity monitoring," *Sensors*, vol. 10, no. 8, pp. 7772–7788, 2010.

[19] P. D. Thompson *et al.*, "Exercise and physical activity in the prevention and treatment of atherosclerotic cardiovascular disease," *Circulation*, vol. 107, no. 24, pp. 3109–3116, 2003.

[20] S. P. Helmrich, D. R. Ragland, R. W. Leung, and R. S. Paffenbarger, Jr., "Physical activity and reduced occurrence of non-insulin-dependent diabetes mellitus," *New England J. Med.*, vol. 325, no. 3, pp. 147–152, 1991.

[21] R. L. Weinsier, G. R. Hunter, A. F. Heini, M. I. Goran, and S. M. Sell, "The etiology of obesity: Relative contribution of metabolic factors, diet, and physical activity," *Amer. J. Med.*, vol. 105, no. 2, pp. 145–150, 1998.

[22] E. M. Tapia, S. S. Intille, and K. Larson, "Activity recognition in the home using simple and ubiquitous sensors," in *International Conference on Pervasive Computing*. Berlin, Germany: Springer, 2004, pp. 158–175.

[23] A. Danielsen, H. Olofsen, and B. A. Bremdal, "Increasing fall risk awareness using wearables: A fall risk awareness protocol," *J. Biomed. Informat.*, vol. 63, pp. 184–194, Oct. 2016.

[24] S.-R. Ke *et al.*, "A review on video-based human activity recognition," *Computers*, vol. 2, no. 2, pp. 88–131, 2013.

[25] J. K. Aggarwal and L. Xia, "Human activity recognition from 3d data: A review," *Pattern Recognit. Lett.*, vol. 48, pp. 70–80, Oct. 2014.

[26] K.-T. Song and Y.-Q. Wang, "Remote activity monitoring of the elderly using a two-axis accelerometer," in *Proc. CACS Autom. Control Conf.*, Tainan, Taiwan, 2005, pp. 18–19.

[27] F. Foerster, M. Smeja, and J. Fahrenberg, "Detection of posture and motion by accelerometry: A validation study in ambulatory monitoring," *Comput. Human Behav.*, vol. 15, no. 5, pp. 571–583, 1999.

[28] A. Mannini and A. M. Sabatini, "Machine learning methods for classifying human physical activity from on-body accelerometers," *Sensors*, vol. 10, no. 2, pp. 1154–1175, 2010.

[29] M. Mathie, B. G. Celler, N. H. Lovell, and A. C. F. Coster, "Classification of basic daily movements using a triaxial accelerometer," *Med. Biol. Eng. Comput.*, vol. 42, no. 5, pp. 679–687, 2004.

[30] L. Atallah, B. Lo, R. King, and G.-Z. Yang, "Sensor positioning for activity recognition using wearable accelerometers," *IEEE Trans. Biomed. Circuits Syst.*, vol. 5, no. 4, pp. 320–329, Aug. 2011.

[31] G. Cohn *et al.*, "An ultra-low-power human body motion sensor using static electric field sensing," in *Proc. ACM Conf. Ubiquitous Comput.*, Pittsburgh, PA, USA, 2012, pp. 99–102.

[32] R. Jafari and R. Lotfian, "A low power wake-up circuitry based on dynamic time warping for body sensor networks," in *Proc. IEEE Int. Conf. Body Sensor Netw.*, Dallas, TX, USA, 2011, pp. 83–88.

[33] E. P. Carden and P. Fanning, "Vibration based condition monitoring: A review," *Struct. Health Monitor.*, vol. 3, no. 4, pp. 355–377, 2004.

[34] O. Z. Olszewski, R. Houlihan, A. Blake, A. Mathewson, and N. Jackson, "Evaluation of vibrational PiezoMEMS harvester that scavenges energy from a magnetic field surrounding an AC current-carrying wire," *J. Microelectromech. Syst.*, vol. 26, no. 6, pp. 1298–1305, Dec. 2017.

[35] N. Jackson, R. O'Keeffe, F. Waldron, M. O'Neill, and A. Mathewson, "Evaluation of low-acceleration MEMS piezoelectric energy harvesting devices," *Microsyst. Technol.*, vol. 20, nos. 4–5, pp. 671–680, 2014.

[36] H. Li, C. Tian, and Z. D. Deng, "Energy harvesting from low frequency applications using piezoelectric materials," *Appl. Phys. Rev.*, vol. 1, no. 4, 2014, Art. no. 041301.

[37] R. J. M. Vullers, R. van Schaijk, I. Doms, C. Van Hoof, and R. Mertens, "Micropower energy harvesting," *Solid State Electron.*, vol. 53, no. 7, pp. 684–693, 2009.

[38] A. Erturk and D. J. Inman, "Electromechanical modeling of cantilevered piezoelectric energy harvesters for persistent base motions," in *Energy Harvesting Technologies*. Boston, MA, USA: Springer, 2009, pp. 41–77.

[39] S. Boisseau, G. Despesse, and B. A. Seddik, "Electrostatic conversion for vibration energy harvesting," in *Small-Scale Energy Harvesting*, Intech, 2012.

[40] S. Boisseau, G. Despesse, T. Ricart, E. Defay, and A. Sylvestre, "Cantilever-based electret energy harvesters," *Smart Mater. Struct.*, vol. 20, no. 10, 2011, Art. no. 105013.

[41] J. M. Lambrecht and R. F. Kirsch, "Miniature low-power inertial sensors: Promising technology for implantable motion capture systems," *IEEE Trans. Neural Syst. Rehabil. Eng.*, vol. 22, no. 6, pp. 1138–1147, Nov. 2014.

[42] J. Yoo, L. Yan, S. Lee, Y. Kim, and H.-J. Yoo, "A 5.2 mW self-configured wearable body sensor network controller and a 12 uW wirelessly powered sensor for a continuous health monitoring system," *IEEE J. Solid-State Circuits*, vol. 45, no. 1, pp. 178–188, Jan. 2010.

[43] D. Figo, P. C. Diniz, D. R. Ferreira, and J. M. Cardoso, "Preprocessing techniques for context recognition from accelerometer data," *Pers. Ubiquitous Comput.*, vol. 14, no. 7, pp. 645–662, 2010.

[44] C.-Y. J. Peng, K. L. Lee, and G. M. Ingersoll, "An introduction to logistic regression analysis and reporting," *J. Educ. Res.*, vol. 96, no. 1, pp. 3–14, 2002.

[45] K.-R. Muller, S. Mika, G. Ratsch, K. Tsuda, and B. Scholkopf, "An introduction to kernel-based learning algorithms," *IEEE Trans. Neural Netw.*, vol. 12, no. 2, pp. 181–201, Mar. 2001.

Hui Huang received the B.Sc. degree in optical information science and technology from Beijing Jiaotong University, Beijing, China, in 2011. He is currently pursuing the Ph.D. degree in mechanical engineering and engineering mechanics at Michigan Technological University, Houghton, MI, USA.

His current research interests include wearable sensor design and data analytics.

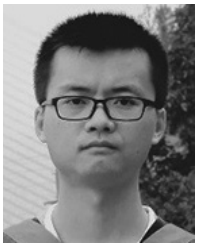

Xian Li received the B.S. degree in biomedical engineering from Tianjin University, Tianjin, China, in 2012, and the M.S. degree in biomedical engineering from Chongqing University, Chongqing, China, in 2015. He is currently pursuing the Ph.D. degree in mechanical engineering at Michigan Technological University (MTU), Houghton, MI, USA.

From 2015 to 2018, he was a Research Assistant with MTU, where he is a Teaching Assistant with the Department of Mechanical Engineering and Engineering Mechanics. His current research interests include human health monitoring during driving via wireless sensor network and energy harvesting based on triboelectrification.

Si Liu received the bachelor's degree in mechanical engineering from Zhejiang University, Hangzhou, China. He is currently pursuing the Ph.D. degree at the Department of Mechanical Engineering and Engineering Mechanics, Michigan Technological University, Houghton, MI, USA.

His current research interest includes the optimization and application of triboelectric energy harvesters.

Shiyan Hu (SM'10) received the Ph.D. degree in computer engineering from Texas A&M University, College Station, TX, USA, in 2008.

He is an Associate Professor with Michigan Technological University, Houghton, MI, USA, where he is the Director of the Center for Cyber-Physical Systems. He was a Visiting Professor with IBM Research, Austin, TX, USA, in 2010, and a Visiting Associate Professor with Stanford University, Stanford, CA, USA, from 2015 to 2016. His current research interests include cyber-physical systems (CPSs), CPS security, data analytics and computer-aided design of very large-scale integration circuits, in which he has authored or co-authored over 100 refereed papers.

Dr. Hu was a recipient of the National Science Foundation CAREER Award, the ACM SIGDA Richard Newton DAC Scholarship (as a Faculty Advisor), and the JSPS Faculty Invitation Fellowship. He is the Editor-in-Chief of *IET Cyber-Physical Systems: Theory and Applications*. He serves as an Associate Editor for the IEEE TRANSACTIONS ON COMPUTER-AIDED DESIGN OF INTEGRATED CIRCUITS AND SYSTEMS, the IEEE TRANSACTIONS ON INDUSTRIAL INFORMATICS, and the IEEE TRANSACTIONS ON CIRCUITS AND SYSTEMS. He is also a Guest Editor of eight IEEE/ACM journals, such as the PROCEEDINGS OF THE IEEE and the IEEE TRANSACTIONS ON COMPUTERS. He is an ACM Distinguished Speaker, an IEEE Systems Council Distinguished Lecturer, an IEEE Computer Society Distinguished Visitor, and an invited participant for the U.S. National Academy of Engineering Frontiers of Engineering Symposium. He is the Chair of the IEEE Technical Committee on Cyber-Physical Systems. He has held chair positions in numerous IEEE/ACM conferences. He is a Fellow of the IET.

Ye Sun (M'14) received the B.S. degree in instrumentation engineering from Tianjin University, Tianjin, China, in 2009, and the Ph.D. degree from Case Western Reserve University, Cleveland, OH, USA, in 2014.

She is currently an Assistant Professor with the Department of Mechanical Engineering and Engineering Mechanics, and an affiliated Assistant Professor with the Department of Biomedical Engineering, Michigan Technological University, Houghton, MI, USA. Her current research interest includes an interdisciplinary resort that integrates engineering innovation with human health and human behaviors.

Dr. Sun is a member of the ASME.